energies

MDPI

Article

Chemostratigraphic Analysis of Wufeng and Longmaxi Formation in Changning, Sichuan, China: Achieved by Principal Component and Constrained Clustering Analysis

Zhifeng Zhang [1,2], Yongjian Huang [1,2,*], Bo Ran [3], Wei Liu [4], Xiang Li [2] and Chengshan Wang [1,2,*]

1 State Key Laboratory of Biological and Environmental Geology, China University of Geosciences, Beijing 100083, China; 3001190101@cugb.edu.cn
2 School of the Earth Science and Resources, China University of Geoscience, Beijing 100083, China; 3001190041@cugb.edu.cn
3 State Key Laboratory of Oil and Gas Reservoir Geology and Exploitation, Chengdu University of Technology, Chengdu 610059, China; ranbo08@cdut.cn
4 Chengdu Center, China Geological Survey, Chengdu 610082, China; liuwei@mail.cgs.gov.cn
* Correspondence: huangyj@cugb.edu.cn (Y.H.); chshwang@cugb.edu.cn (C.W.)

Abstract: The increasing proportion of unconventional worldwide energy demands have consistently promoted the necessity for exploring a precise, high-resolution, objective, and quantitative stratigraphic division method for macroscopically homogeneous mudstone successions. The chemostratigraphy can resolve this problem well, although it has been applied successfully in North America, but not systematically studied in China for shale gas exploration and development. This work has conducted a chemostratigraphic analysis of Wufeng and Longmaxi Formation on the Changning section of Sichuan Province, southwestern China, to testify its applicability for shale gas exploration in China. Principal component analysis (PCA) was first employed to reduce the dimensionality of datasets. Three chemofacies, including detrital (K, Ti, Fe, Al, Na, Mg, Cr, Zr, Rb), authigenic (Ca, Sr, Mn, Si, S, Ba), and redox-organic (P, V, Ni, Zn, Cu, TOC), were found. Subsequently, constrained clustering analysis was utilized for the zonation of each chemofacies into chemozones. Consequently, the whole Changning section was divided into twelve chemozones (CZ I–CZ XII). The geochemical interpretation for these chemozones can be resolved from the regional changes in paleogeography and paleoceanography during the Late Ordovician to Early Silurian period. Thus, a three-stage geochemical evolution along the Changning section can be classified: (1) the siliceous and anoxic deposits of Wufeng Formation (CZ I–CZ III) with high TOC contents; (2) the siliceous and anoxic sedimentary rocks of bottom Longmaxi Formation with still higher TOC (CZ IV); (3) the calcarous-detrital and oxic sediments for the rest of Longmaxi Formation (CZ V–CZ XII). In considering their high content of TOC and abundant brittle siliceous minerals, the CZ (I–IV, 0 m–33.6 m) are thought to be the most preferable sweet spot for shale gas exploration.

Keywords: Wufeng-Longmaxi Formation; geochemistry; chemofacies; chemozones; sweet-spot layers

check for updates

Citation: Zhang, Z.; Huang, Y.; Ran, B.; Liu, W.; Li, X.; Wang, C. Chemostratigraphic Analysis of Wufeng and Longmaxi Formation in Changning, Sichuan, China: Achieved by Principal Component and Constrained Clustering Analysis. *Energies* **2021**, *14*, 7048. https://doi.org/10.3390/en14217048

Academic Editor: Alireza Nouri

Received: 14 July 2021
Accepted: 20 October 2021
Published: 28 October 2021

Publisher's Note: MDPI stays neutral with regard to jurisdictional claims in published maps and institutional affiliations.

Copyright: © 2021 by the authors. Licensee MDPI, Basel, Switzerland. This article is an open access article distributed under the terms and conditions of the Creative Commons Attribution (CC BY) license (https://creativecommons.org/licenses/by/4.0/).

1. Introduction

The production of unconventional energy, especially shale gas, has increased dramatically in recent years to satisfy the growing demand for energy worldwide [1]. The precise and high-resolution stratigraphic division and correlation of mudstone successions has become one of the most important steps in exploration and development of shale gas [2]. However, the macroscopically homogeneous attributes and limited fossil constraints of shales hinder the availability of biostratigraphy and lithostratigraphy [3]. Moreover, the lack of seismic, drilling, and logging data [4] as well as the difficulty in identifying distinct facies shifts [5] within such rocks disable the efficiency of seismic, well logging, and sequence stratigraphic techniques [6–10]. New methodologies are needed to give a reliable and high-resolution stratigraphic scheme for shale gas exploration.

Fortunately, chemostratigraphy, which divides and correlates the succession based on the subtle variations in the elemental composition of the sediments, can deal with this matter quite well and has been applied widely and successfully for developing unconventional oil and gas in North America [9–16]. The rationale behind this fact is that the heterogeneity of macroscopically homogeneous mudstones can be best resolved by the chemical composition, which may reflect the climate variation in the source region, productivity in the ocean surface, and redox change at the bottom water, or even the hydrothermal input into the sediments [10,11,17–20]. For these reasons, chemostratigraphy has become one of the most preferable stratigraphic division methods for mudstone successions [18]. Besides, the multivariate-statistically based chemostratigraphic technique is a new trend that can provide more objective and quantitative results [4,10,20,21].

China is the first country that has commercialized shale gas development outside of North America. The Ordovician Wufeng (O_3w) and Silurian Lomgmaxi (S_1l) Formation are the main reservoirs which distribute widely in southwestern China, especially in Sichuan Province. Though much progress has been made regarding the establishment of shale-gas developing technologies compatible with Chinese geology [22–24], chemostratigraphic study has not been done systematically in these two Formations. Thus, this work conducts a chemostratigraphic analysis of Changning section, one of the most frequently studied sections for Wufeng and Longmaxi shales in China, to obtain a high-resolution and precise stratigraphic scheme for these two Formations and identify the sweet-spot layers for exploration, ultimately promoting the application of this method to Chinese shale-gas exploration.

2. Geological Setting

The Sichuan Basin in southwestern China is an intracontinental depression basin that occurred during the Late Ordovician to Early Silurian period [25] and is tectonically located in northwestern portion of the Yangtze Platform. Under the action of synchronous Caledonian orogeny during the Late Ordovician period, the target area is surrounded by central Sichuan paleouplift in the north, central Guizhou paleouplift in the south, and Xuefeng paleouplift in the east [26,27] (see Figure 1 for details), which results in a restricted and semi-enclosed continental shelf sedimentation condition [28] under which a set of graptolitic black shales of Wufeng Formation was deposited [29]. At the last phase of the Late Ordovician (Hirnantian), extensive global regression [30] occurred which was caused by the Gondwana glaciation event, and the Brachiopod-developed limestone of the Guanyinqiao Layers was deposited on the top of the Wufeng Formation. Until the Early Silurian period, due to the effect of volcanic and global warming deglaciation commenced and the resulting transgression of seawater [31] contributed to the deposition of deep-shelf black shales of the Lower Longmaxi Formation [32]. After that, the later constant shallowing event ultimately led to the formation of silty shales of middle-upper Longmaxi [24,26].

Changning section, located in Changning County of Sichuan Province, southwestern China, is situated at the paleo-depocenter of the Wufeng and Longmaxi Formation. This section is one of the most typical profiles for studying Wufeng and Longmaxi shales in China [24,26,33]. Here the Wufeng Formation (O_3w) is characterized by laminated and massive siliceous shales with *Orthograptus* fossils, and the siliceous radiolaria is visible under microscopes [33]. As for the Longmaxi Formation (S_3l), its lower parts are comprised of black and carbonaceous shales, with lamina and *Orthograptus* fossils well developed in the strata. In the middle and upper part of the Longmaxi Formation, silty shales and mudstone are the dominate lithological types with *Rastrites* fossils at the top, which indicates a much shallower deposition condition [26,33].

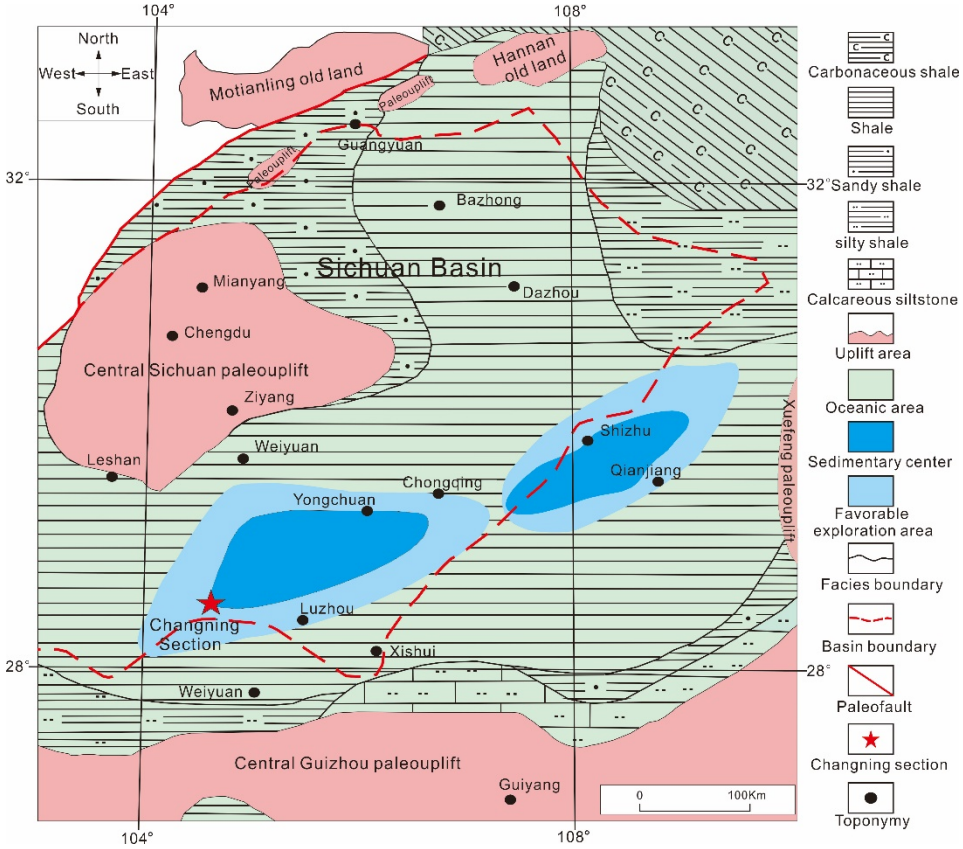


Figure 1. Paleogeographic map of Yangtze platform during the Late Ordovician to Early Silurian period (Modified after [26]).

3. Materials and Methods

3.1. Materials

In this study, we took the Changing section as the research subject, which is tectonically located in the Upper Yangtze area. Wufeng and Longmaxi Formation outcrop well in this section, with a thickness of more than 300 m. In total, 87 geochemical samples, with a majority sampling interval of approximately 0.5 m, were collected from Wufeng to Longmaxi Formation. The total sampled thickness was about 170 m and the biostratigraphy of Wufeng and Longmaxi Formation was considered according to [34]. Surface layers were excavated out to ensure that fresh samples were taken without alteration. Then all the samples were ground into powder for geochemical analysis.

The contents of main and trace elements of samples were measured by Wavelength Dispersive X-ray Fluorescence Spectrometer (XRF) in Microstructure Analysis Laboratory of Beijing. The major elements, including K, Ti, Fe, Ca, Mn, Si, Al, P, Na and Mg, are measured as a percentage of metallic oxides, and the trace elements, including V, Cr, Ni, Zn, Cu, Sr, S, Zr, Rb, Ba and Cl, are expressed in mg/kg. Calibration was done with 25 rock reference materials (GBW07101-07125) certified by the Chinese Academy of Geological Sciences. Total organic carbon (TOC), expressed in percentage by weight (%), was measured in a total carbon and total nitrogen analyzer of Jena TOC/TN Multi NC2100S, in the laboratory at Academy of Science, China University of Geosciences at Beijing. The whiting was used to calibrate the machine. For convenience, various of units are expressed as mg/kg to avoid the multivariate statistical analysis error [20]. The datasets for the geochemical measurements are documented in Table A1.

3.2. Multivariate Statistical Techniques

The implementation of chemostratigraphy is never easy work, though it is, without doubt, an effective method for shale gas exploration [11]. The most important step in the

chemostratigraphy is how to realize the zonation of the geochemical data/curves (when presented in a figure) in a reasonable way which results in a reliable and interpretive stratigraphic scheme for the studied succession [9–11,13,14,18,20,35]. Furthermore, the compositional data of these successions are high-dimensional in nature which makes the work even more difficult [10]. For example, the dataset of Changning section, presented here and determined by XRF, includes more than 20 elemental contents of 87 samples. Traditionally, the zonation of geochemical data/curves has been conducted in an artificial way which was subjectively affected by the experience and knowledge of the operator. Then, automatic zonation by software programs, especially multivariate statistical techniques, was introduced [36]. However, the analysis of chemostratigraphic data is not without principle when utilizing multivariate statistical techniques [37]. In this work, the dimension of the chemostratigraphic dataset needs to be reduced firstly to the items of the data combined with new variables of specific geochemical meaning by principal component analysis (PCA), and then the zonation of the new variables, for example, by constrained clustering analysis, can be conducted. In this sense, these steps are quite similar to those of zonation of well-logging curves [38]. Detailed steps of chemostratigraphic analysis are elaborated below.

3.2.1. Principal Component Analysis

Principal component analysis (PCA) is a commonly used technology in many disciplines for reducing the dimensions of a dataset [37,39]. The philosophy of this technique is to transform the massive variables of the dataset into several principal components while preserving the majority of the information of the original dataset [39]. For sedimentary geochemical data reduction, this method can group the elements into several principal components, and the geochemical meaning of each component is defined and interpreted by the respective elemental association [40]. Usually, the geochemical behavior of each element association is somewhat different and therefore can define certain geochemical properties of the sedimentary environment, i.e., each principal proponent/element association may stand for a certain type of chemical facies (chemofacies) of sedimentary environment according to the definition [18,36,41]. For example, Montero-Serrano et al. (2010) grouped the whole-rock elemental data using PCA into the detrital, authigenic, and redox chemofacies, in order to conduct chemostratigraphic analysis [20]. In a geochemical perspective, the composition of fine-grained sedimentary rocks usually come from detrital, authigenic, redox, bioproductivity, etc., which can be identified by the PCA [42,43]. In this sense, we think the data reduction process of the chemostratigraphic dataset is the same process for the identification of chemofacies by PCA [44,45].

3.2.2. Constrained Clustering Analysis

The constrained clustering analysis is a multivariate statistical approach for sorting the data plotted in a higher-dimensional space without disorganizing their original sequences based on the degree of similarity quantified by the distance between two adjacent 'clusters' [10]. For the geological samples, they are arranged according to the stratigraphic depth (in meters) in the dendrogram which vividly displays the result of constrained clustering analysis in the form of a graphic [38]. 'Manhattan Distance' and 'Euclidian Distance' are the two most commonly used methods to measure distance. Considering that possible correlations may exist among variables of rock samples, 'Euclidian Distance' is thought to be more proper for its assumption that certain dependence is allowed among variables [10], thus, the length of the straight line between two clusters is employed to quantify the degree of similarity. Each cluster is represented by the center of the cluster, which means that the 'K-means method' is used. Then the newly merged clusters are defined using 'Ward's method' or the minimum variance of the original cluster, which maximize the difference between two clusters and minimize the difference within clusters [5,9,46,47]. Accordingly, 'K-means method', 'Euclidean distance', and 'Ward's method' were chosen for constrained clustering analysis to realize the division of succession. Furthermore, the ultimate number

of clusters depends on the selection of cutoff values in the dendrogram [20,48]. The data quality is also vitally important for chemostrtigraphy. The presence of irregular data, especially zeroes and outliers, will make it difficult for data analysis [49,50]. Fortunately, no such data were represented here, therefore the pre-treatment step was ignored. PCA and constrained clustering analysis were conducted using SPSS Statistic 19 software and Rioja package (in R), respectively, in this work.

4. Results

4.1. Identification of Chemofacies

The principal component analysis was conducted to reduce the dimension, and also for the identification of chemofacies of Wufeng and Longmaxi Formation in Changning section. As is shown in Table 1, three principal components (PCs) can be identified corresponding to three elements associations, i.e., PC1 to element association 1 (K, Ti, Fe, Al, Na, Mg, Cr, Zr, Rb), PC2 to element association 2 (Ca, Mn, Si, Sr, S, Ba), PC3 to element association 3 (P, V, Ni, Zn, Cu, TOC). The spatial distribution of the loading of 22 elements shows three elemental associations as well (Figure 2). Due to its small loading components (<0.1) at each principal factor, Chlorine (Cl) cannot be grouped into any one of them.

Element associations of sedimentary rocks, as represented by each principal component, are the comprehensive products of the weathering, transportation, and deposition process. Thus, thereafter we call these element associations chemofacies. The geological meanings of the chemofacies (element associations) can be interpreted as below:

Table 1. The loading table of principal components.

Elements	PCA1	PCA2	PCA3	Elements	PCA1	PCA2	PCA3
K	0.94	−0.13	−0.30	Cr	0.60	−0.24	−0.19
Ti	0.92	−0.08	−0.24	Ni	−0.34	−0.04	0.75
Fe	0.86	0.13	−0.06	Zn	−0.21	−0.12	0.53
Ca	−0.35	0.93	−0.07	Cu	−0.43	−0.12	0.50
Mn	−0.07	0.84	−0.18	Sr	−0.27	0.93	−0.08
Si	−0.47	−0.88	0.11	S	0.01	0.54	−0.01
Al	0.93	−0.13	−0.33	Zr	0.42	−0.09	−0.14
P	−0.19	0.06	0.62	Rb	0.83	−0.13	−0.26
Na	0.67	0.08	−0.29	Ba	0.11	0.32	−0.29
Mg	0.79	0.33	−0.40	Cl	0.08	−0.08	0.10
V	−0.41	−0.15	0.53	TOC	−0.33	−0.19	0.92

(a) Chemofacies 1 (K, Ti, Fe, Al, Na, Mg, Cr, Zr, Rb) mainly consists of elements that originated from the provenance region of sediments. Among these elements, K, Al, Rb, and Fe are the main chemical components of fine detrital minerals [51,52], in particular clay minerals and iron oxides. Cr is vulnerable to be absorbed by clay minerals, thus it is preferable to be preserved in finer parts of mudstone [42]. On the contrary, Na, Mg, Ti, and Zr may be related to the coarse component of terrestrial inputs and hosted in feldspar, rutile, and zircon [42]. Consequently, this chemofacies can reflect both the proportion of detrital materials and even the ratio of coarse: fine minerals within rocks, and ultimately be interpreted as detrital chemofacies (DT).

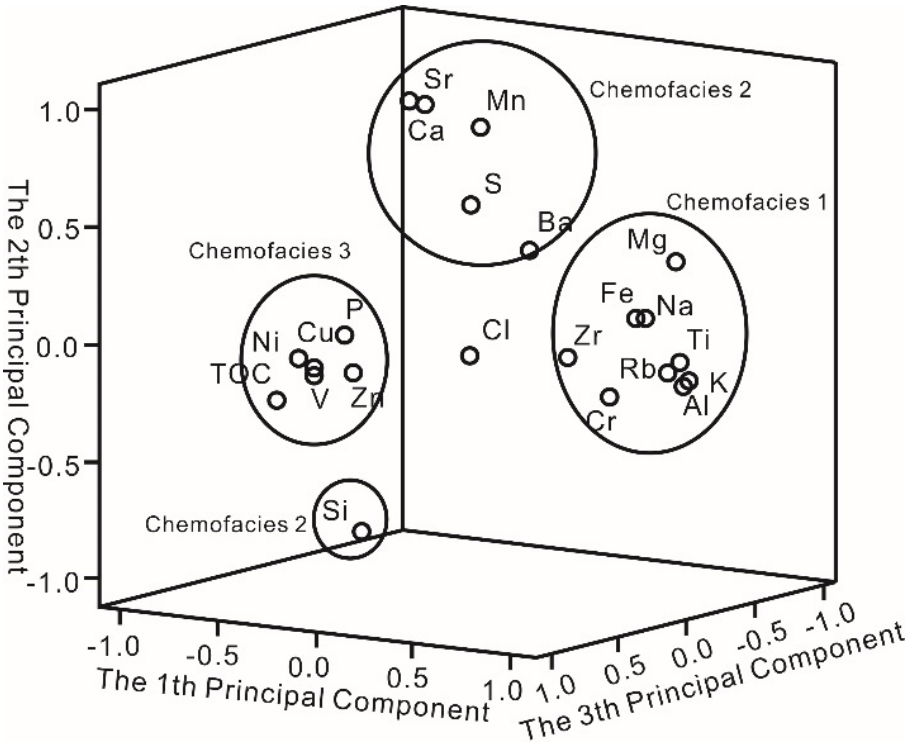


Figure 2. The spatial distribution of principal component loading of 22 elements.

(b) Chemofacies 2 (Ca, Sr, Mn, Si, S, Ba) is mostly comprised of authigenic elements sourced from carbonates and siliceous depositions and can be regarded as an authigenic chemofacies (AT). It is well-known that element Ca and Sr are associated with carbonate minerals in marine settings. Mn can occur as $MnCO_3$, resulting from the reduction of manganese oxides in the reduction environment [51,53], which is consistent with the deposition environment indicated by the black shales. The high correlation between barium and sulfur within this association may imply that both elements forming the barite as the organic matter were oxidized by the sulfate. Besides, sulfur can also deposit in the form of pyrite [51]. However, the most striking feature of this association is that element Si shows a high negative loading. Si often shows multiple sources, such as terrestrial input and biogenic influx. Based on the evidence from the thin section under microscopes, the silicon content of the Changning section may be primarily made up of the biogenic production of siliceous organism, which can be approved by the occurrence of radiolarias, indicating a nutrient-rich condition [26,42].

(c) Chemofacies 3 (P, V, Ni, Zn, Cu, TOC) is comprised of redox-sensitive elements which are closely related to the productivity and preservation of organic carbon, thus can be interpreted as redox-organic chemofacies (RO). This association contains two meanings, the first one refers to the nutrient-related elements such as P, Zn, Cu; the other one is the redox-sensitive elements which will be absorbed into depositions under reduction bottom water conditions, such as V and Ni [41,54–59]. The TOC is the comprehensive product of these two aspects.

The total variance explained by these three principal factors/element associations/chemofacies is 63.21%, 30.76%, and 5.05%, respectively. This means that the variations of chemofacies of DT, AT, RO (PC1, PC2, and PC3) can represent the main basis for characterizing the chemostratigraphy of Wufeng and Longmaxi Formation in the Changning section [60].

4.2. Zonation of Chemofacies

Once the main chemofacies (element associations) for the section were established, the constrained clustering analysis could be employed to obtain a number of distinctive chemozones. The zonation of chemofacies resulted from the dendrograms and depended on the selection of cut-off value [38]. The choice of this value must be based on regional geological settings. Accordingly, 690, 1700, and 810 cut-off values were chosen, respectively, for the zonation of the detrital, authigenic, and redox-organic chemofacies. Three dendrograms derived from the constrained clustering analysis based on chemofacies can be seen in Figure A1. Therefore, the zonation results of the three chemofacies were determined as follows:

(1) In view of DT chemofacies, the section (Wufeng and Longmaxi Formation) can be divided into nine chemozones from bottom to top, i.e., DTI (0 m–3.0 m), DTII (3.0 m–4.3 m), DTIII (4.3 m–8.8 m), DTIV (8.8 m–33.6 m), DTV (33.6 m–39.4 m), DTVI (39.4 m–67.0 m), DTVII (67.0 m–104.5 m), DT VIII (104.5 m–115.7 m) and DTIX (115.7 m–170 m) (Figure 3).

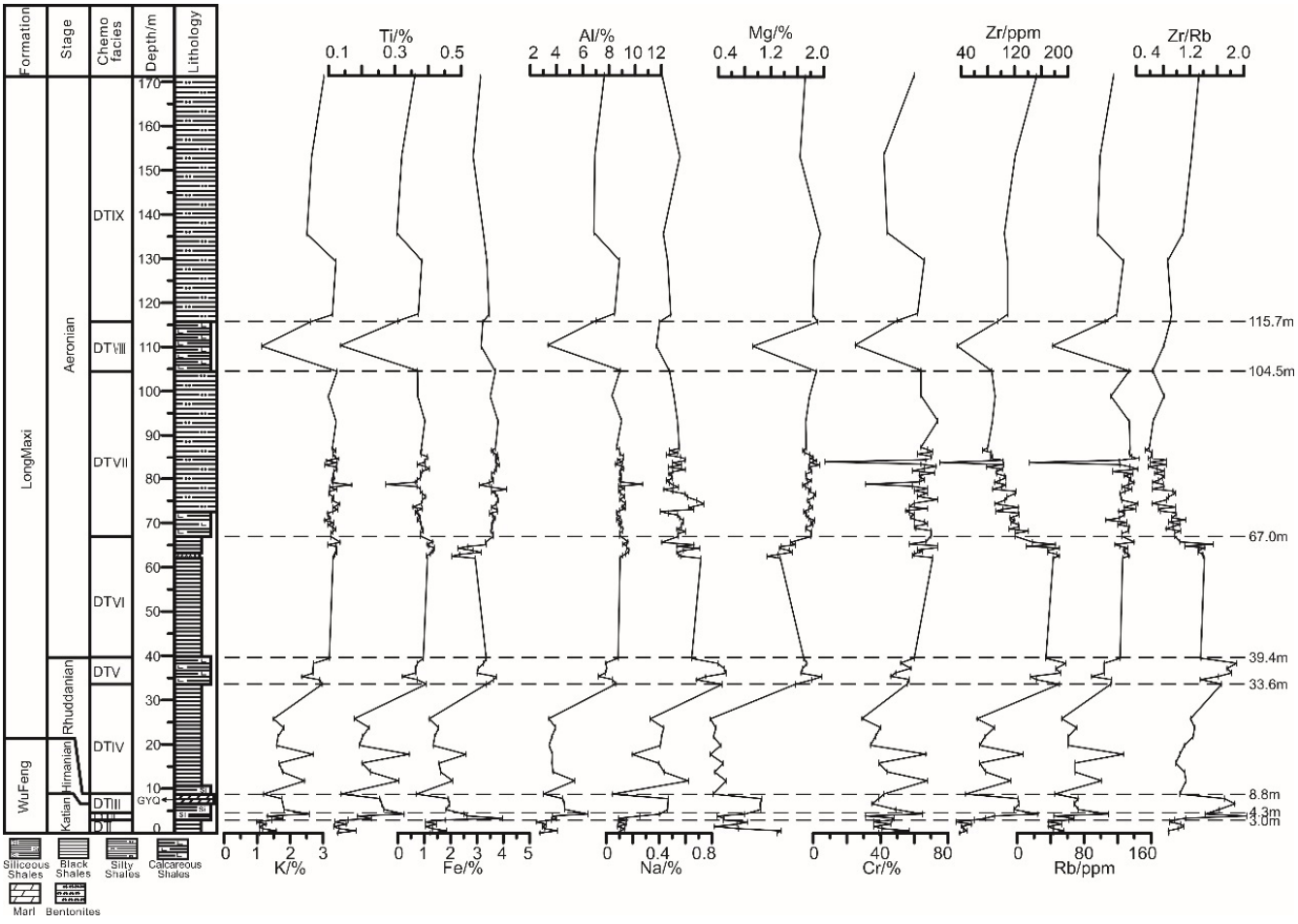


Figure 3. The chemozones based on detrital chemofacies of the Changning section.

(2) The same number of chemozones were discerned for the AT chemofacies, including ATI (0 m–3.0 m), ATII (3.0 m–4.3 m), ATIII (4.3 m–8.8 m), ATIV (8.8 m–33.6 m), ATV (33.6 m–62.0 m), ATVI (62.0 m–67.0 m), ATVII (67.0 m–72.6 m), ATVIII (72.6 m–98.8 m) and ATIX (98.8 m–170 m) (Figure 4).

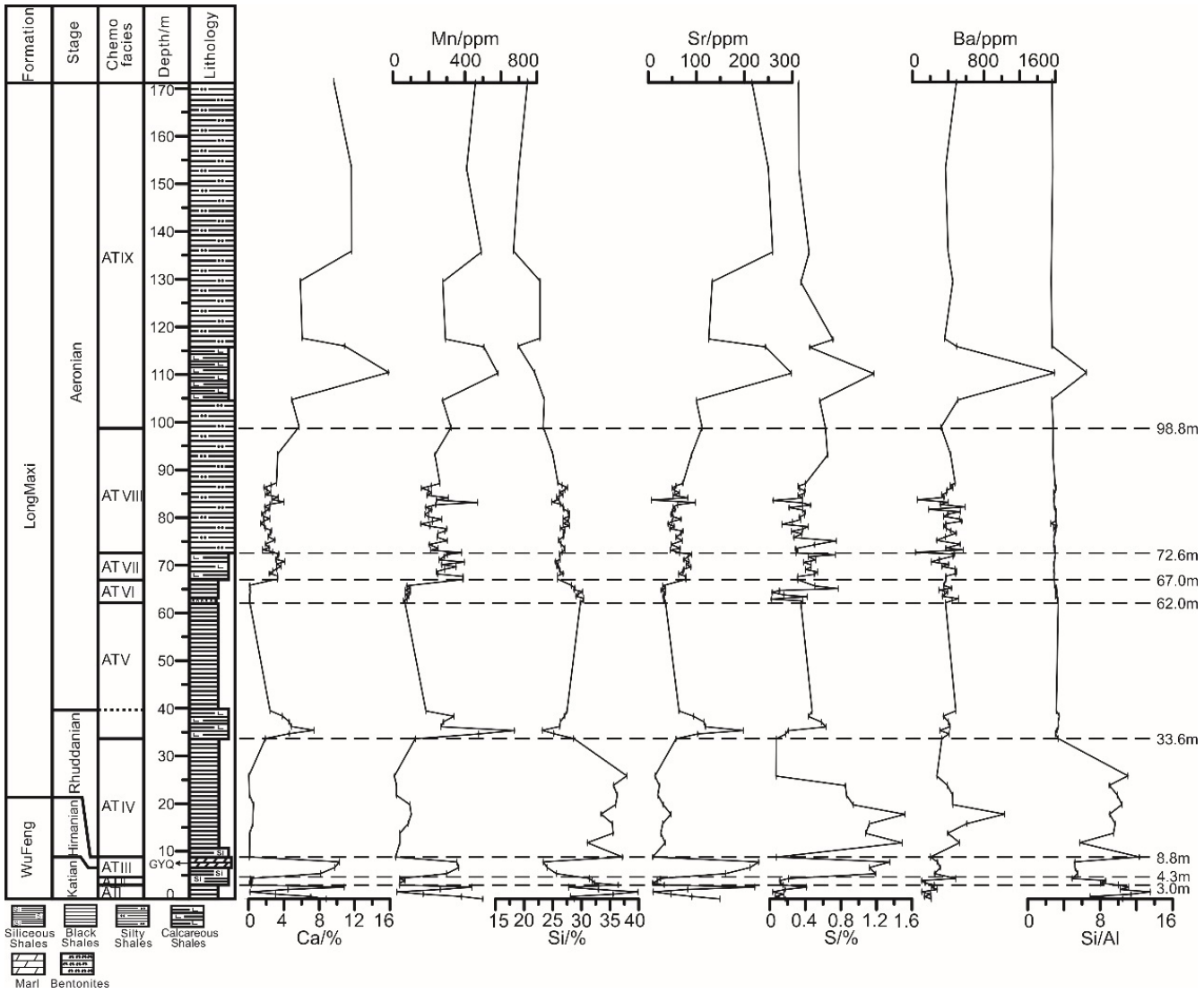


Figure 4. The chemozonation based on authigenic chemofacies of the Changning section.

(3) The target succession of Wufeng and Longmaxi Formations was partitioned into five chemozones according to the variation of the redox-organic element association, i.e., ROI (0 m–3.0 m), ROII (3.0 m–4.3 m), ROIII (4.3 m–8.8 m), ROIV (8.8 m–33.6 m) and ROV (33.6 m–170 m) (Figure 5).

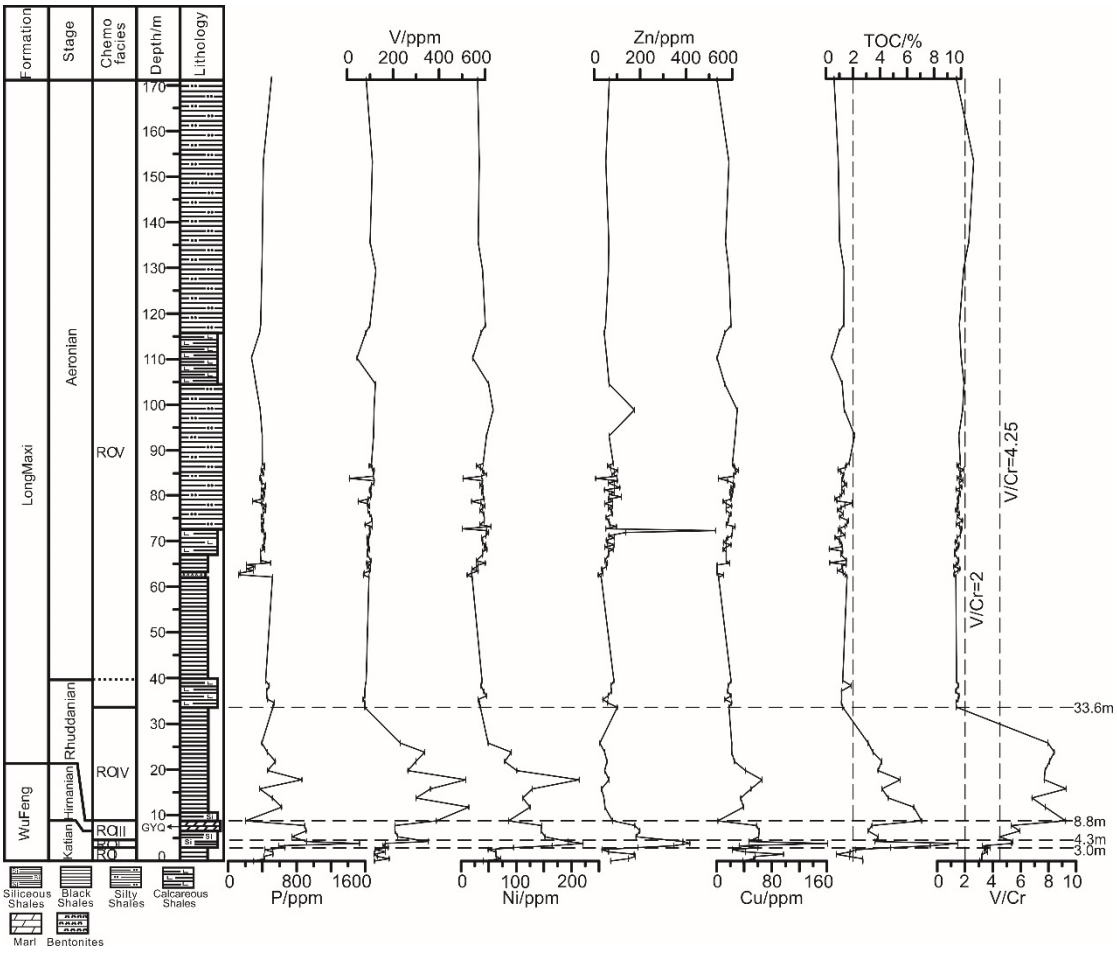


Figure 5. The chemozonation based on redox-organic chemofacies of the Changning section.

5. Discussion

Wufeng and Longmaxi Formations are always the most important successions for shale gas exploration in China, and many works have been done on the Changning section [22–24]. Wang et al. (2014) and Dong et al. (2010) [60,61] studied TOC contents and geochemistry of major elements for the section and thereafter thought that Wufeng and lower Longmaxi Formations, deposited in a deep shelf environment, are the preferable layers for shale gas exploration. Luo et al. (2017) [33] focused on biostratigraphic analysis, with the conclusions that the sequences at the top of Wufeng Formation and the bottom of Longmaxi contain the graptolite zone of *Dicellograptus complexus-Coronograptus cyphus* which is an indicator of the sweet spot. Zhou (2015) and Zhang et al. (2013) [27,62] considered the geochemical characteristics of the Longmaxi Formation, which also indicated that the lower Longmaxi was deposited under anoxic conditions and showed higher potential for organic matter preservation than that of the middle and upper Longmaxi. However, the recognition of optimal shale gas layers is still descriptive and qualitative in all these listed works. Thus, this work aimed to resolve this problem in a more quantitative manner based on the chemostratigraphic technique to promote shale gas exploration in Wufeng-Longmaxi Formations.

5.1. Interpretation of Zonation of Chemofacies

5.1.1. The Detrital Chemofacies

As it is shown in Figure 3, the fluctuations of detrital associations in the section coincided with each other but are opposite to that of carbonaceous–siliceous elements (Figure 4). For example, at intervals of 52.1 m–41.9 m, the contents of K, Ti, Al, Rb and Cr

show a sudden decreasing trend (Figure 3), while the content of Ca shows a corresponding increasing excursion (Figure 4). This situation indicates that the two components are the basis for the chemostratigraphic analysis of the section, as stated above. The detailed comparison between division results of detrital chemofacies and changing trends of these detrital elements along the section are shown below:

(1) The contents of the detrital elements of DT I (0 m–3.0 m) are generally low and stable, indicating constantly low terrigenous inputs during this period;
(2) At DT II (3.0 m–4.3 m), the content of the detrital association is still low, but with a slowly increasing tendency, representing a low but progressive increase in debris input;
(3) For DT III (4.3 m–8.8 m), the contents of fine component of detrital elements (K, Fe, Al, Rb, Cr) are low but the coarse fractions are high (Ti, Na, Mg, Zr), reflecting a decrease in sea level;
(4) The content of the detrital elements at DT IV (8.8 m–33.6 m) is higher than DT III but lower than DT V (33.6 m–39.4 m), representing a progressive increase in terrigenous input;
(5) The detrital inputs at DT V (33.6 m–39.4 m) are generally high. In more detail, the fine fraction is low compared with relatively high coarse components;
(6) The content of detrital elements at DT VI (39.4 m–67.0 m) intervals is high overall. In detail, Zr, as the indicator of coarse debris, drops slightly, while other elements with the meaning of fine debris show a slightly increasing trend, indicating higher terrigenous inputs caused by regression;
(7) At DTVII (67.0 m–104.5 m), the contents of detrital elements are high but with slight fluctuations, as approximately mirrored by that of authigenic chemofacies, which indicates mutual dilution between detrital and authigenic chemofacies (see Figures 4 and 5);
(8) The contents of detrital elements are significantly reduced at DT VIII (104.5 m–115.7 m). Combined with the high contents of carbonate-related elements during this interval (see Figure 4), it is believed that the terrigenous influxes are high and affected by carbonate dilution of seawater during this period;
(9) At DT IX (115.7 m–170 m), the element contents of detrital return to a relatively high and stable level, indicating no significant changes in terrigenous inputs compared with that at DT VIII.

5.1.2. The Authigenic Chemofacies

The authigenic chemofacies are principally of authigenic origin from carbonate and siliceous deposition. Ca, Mn, Sr, S, Ba reflect the calcareous minerals within the strata. Si is mainly derived from the biogenic input, though some belong to detrital sources [26,42]. It is worth mentioning that the minus loading component (−0.88 loading, detailed in Table 1) of Si in this association means mutual dilution between calcareous and siliceous matters, which indicates the alternative deposition of these two kinds of minerals, signifying deposition environments with different nutrient levels. Eutrophic conditions are usually for siliceous deposits, and carbonate producers prefer more oligotrophic waters [26,42].

To assess the effect of a determination of chemozone based on the authigenic element association on the stratigraphic division, the detailed correlation between chemozone and changing trends of authigenic association on the section is bound to be implemented:

(1) The contents of Ca, Mn, Sr, S, Ba at AT I (0 m–3.0 m) show a reverse trend against that of Si, constructing a valley on the former curves and a peak on the latter, which makes this zone siliceous sediment;
(2) A high content of Si is sustained at AT II (3.0 m–4.3 m) which contains extremely low contents of Ca, Mn, Sr, S, Ba;
(3) The curves of Ca, Mn, Sr, S, Ba form a bulge, while the Si curve forms a concave at chemozone AT III (4.3 m–8.8 m). The peak of calcareous sediments corresponds to the Guanyinqian Layer, indicating a significant decrease in sea level under the effect of global glaciation during this period [30];

(4) Later, the contents of Ca, Mn, Sr are sustained at a very low level at the lower part of AT IV (8.8 m–33.6 m) and then increase gradually to the upper part, while the content of Si shows a completely contrary trend. It is noteworthy that the trend of Ba and S is the same as that of Si at this chemozone. In consideration of the paleo-productivity implication of Ba, the positive correlation between Ba and Si suggests that biogenic silica producers must be the main contribution to the organic production under nutrient-rich conditions, which is consistent with the significant marine transgression during Rhuddanian [31];
(5) High Ca, Mn, Sr, S, Ba and low Si lead to more calcareous sediments at the bottom of AT V (33.6 m–62.0 m), but then show an opposite trend;
(6) In the interval between 62.0 m and 67.0 m, AT VI, Ca, Mn, Sr, S, Ba are extraordinarily low, but Si is relatively high and stable, which may be due to the increase in detrital inputs (Figure 3).
(7) The contents of Ca, Mn, Sr, S, Ba increase again with a slightly decrease in Si at AT VII (67.0 m–72.6 m);
(8) At AT VIII (72.6 m–98.8 m), the contents of Ca, Mn, Sr, S, Ba decrease again but with subtle fluctuations, which reflects the influence of detrital input, while the content of Si is kept stable;
(9) The contents of Ca, Mn, Sr, S, Ba fluctuate significantly at the lower part, but decrease consistently at the upper part of AT IX (98.8 m–170 m), reflecting the mutual dilution effect between detrital input and authigenic influx when compared with detrital chemozones (Figure 3). The variation of Si is the same as that of detrital input as a whole, indicating no significant biogenic silica input (Figure 3).

5.1.3. The Redox-Organic Chemofacies

Among this element association, V, Ni, Zn, Cu mainly accumulate under reduction conditions, which makes these elements important redox proxies [51,56]. For example, V/Cr ratio is a good redox indicator, with $V/Cr < 2$, $2 < V/Cr < 4.25$ and $V/Cr > 4.25$ corresponding to oxic, suboxic, and anoxic conditions, respectively [63]. Element P and TOC are two of the most important paleo-productivity proxies for ancient lakes and oceans [54,55].

According to the V/Cr ratio in Figure 5, the lower part (0 m–33.6 m) of the Changning section was deposited under an anoxic-suboxic condition, while the oxic condition was dominant during its later interval (33.6 m–170 m). The fact that the relatively high contents of redox-sensitive elements, TOC and P, were in the lower part of the section all together suggests the same conclusion. The zonation results of redox-organic chemofacies and changing trends of element association on the section were compared in detail:

(1) The gradually increase in P, V, Ni, Zn, Cu, TOC, and V/Cr suggests a gradual suboxidation of bottom water during the deposition of RO I (0 m–3.0 m);
(2) At RO II (3.0 m–4.3 m), the content of P, V, Ni, Zn, Cu, TOC reaches a maximum with a local peak at the V/Cr ratio, indicating an anoxic condition and higher productivity;
(3) Most of the elements show a decreasing trend from the bottom to the top of RO III (4.3 m–8.8 m), while the TOC and V/Cr ratio are still high, suggesting anoxic conditions and high paleoproductivities;
(4) The contents of redox-sensitive elements, TOC, and the V/Cr ratio are very high at the lower and middle part of RO IV (8.8 m–33.6 m), but decrease gradually towards the top of this chemozone, implying the anoxic to suboxic bottom-water condition and high productivity;
(5) At ROV (33.6 m–170 m), the content of redox-organic element association maintains at a lower level than that of RO IV, which indicates that this chemozone was deposited under the oxic and low-paleoproductivities condition.
(6) The chemozones results of the three chemofacies described above all show an abrupt shift at the horizontal depths of 33.6 m and 8.8 m, which indicates that variations in sedimentation condition indeed occurred before and after these depths.

5.2. The Unified Chemostratigraphic Scheme and Paleoenvironmental Interpretation

Based on the zonation of each chemofacies, the unified chemostratigraphic scheme can be acquired for the Wufeng and Longmaxi Formation of the Changning section. Ultimately, the Changning section can be divided into twelve Chemozones: CZ I (0 m–3.0 m), CZ II (3.0 m–4.3 m), CZ III (4.3 m–8.8 m) for the Wufeng Formation; CZ IV (8.8 m–33.6 m), CZ V (33.6 m–39.4 m), CZ VI (39.4 m–62.0 m), CZ VII (62.0 m–67.0 m), CZ VIII (67.0 m–72.6 m), CZ IX (72.6 m–98.8 m), CZ X (98.8 m–104.5 m), CZ XI (104.5 m–115.7 m), CZ XII (115.7 m–170 m) for the Longmaxi Formation (Figure 6). This unified chemostratigaphic scheme is easy to understand because the geochemical meaning of each chemozone has been explained in detail in previous sections.

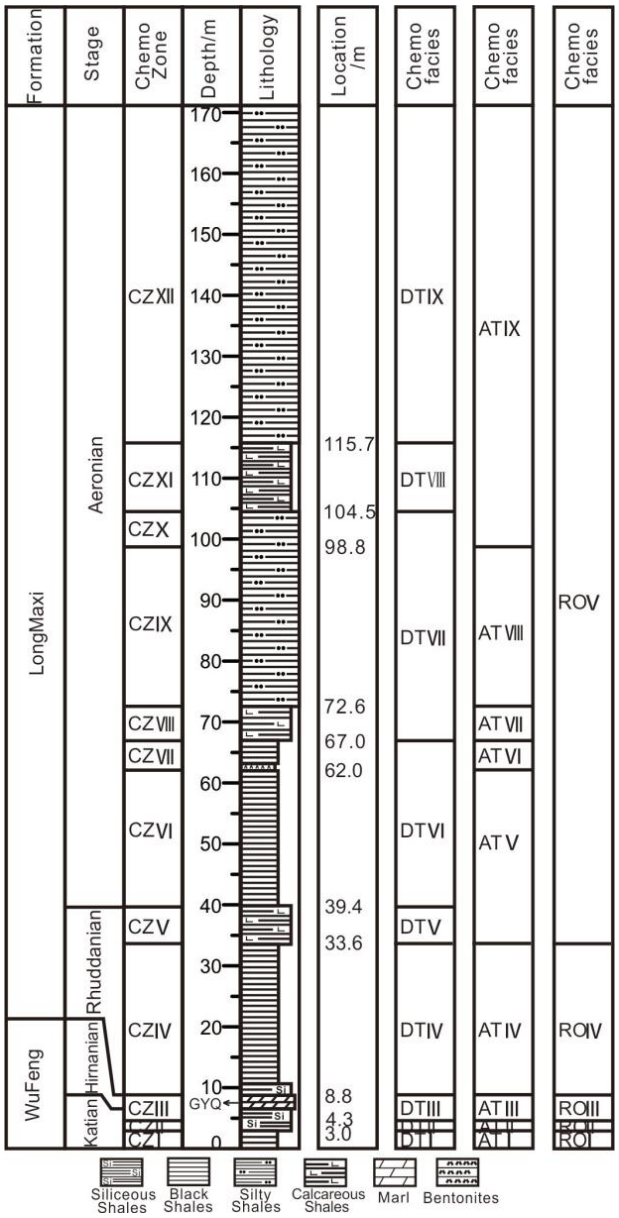


Figure 6. The unified chemostratigraphic scheme of the Changning section.

The geochemical evolution of the Wufeng and Longmaxi Formation on the Changning section is quite variable according to the analysis of each chemofacies. A three-stage of geochemical evolution along the Changning section can be classified, i.e., (1) the siliceous and anoxic deposits of the Wufeng Formation (CZ I–CZ III; 0 m–8.8 m) with high TOC contents,

(2) the siliceous and anoxic sedimentary rocks of the bottom of the Longmaxi Formation with even higher TOC (CZ IV; 8.8 m–33.6 m), (3) and calcareous-detrital and oxic sediments of the rest of the Longmaxi Formation (CZ V–CZ XII; 33.6 m–170 m). It is fascinating that the geochemical evolution can coincide approximately with the biostratigraphic stage as well [34], i.e., CZ (I–III) for Late Katian to Hirnaian, and CZ IV for Rhuddanian and CZ (V–XII) for Aeronian, respectively (Figure 6). The interpretation of these evolution stages can be decoded from the perspective of paleogeographic and paleoceanographic evolution of this region during the Late Ordovician to Early Silurian period [64].

During the Late Ordovician to Early Silurian period, this region was located on the continental shelf of Yangtze platform with a relatively restricted/semi-closed deposition condition and was surrounded by several paleouplifts in the north and south due to the Caledonian orogeny [26,27] (see Figure 1 for details). Only the northeastern-southwestern wards opened to the ocean [28]. The sea level was relatively high, and the sedimentary environment was euxinic, which leads to the deposition of organic-rich Wufeng Formation (CZ I–CZ III) during the Katian period. The sea level then decreased quickly due to the global glaciation at Hirnantian, with the occurrences of shallow-water calcareous facies of Guanyinqiao Layers (top of CZ III).

Marine transgression occurred due to the melting of polar glaciers and tectonic activities at the Yangtze platform [27,65] during the Rhuddanian period. This region revolutionized into a deep shelf; thus, under this anoxic environment the bottom Longmaxi Formation (CZ IV), characterized by high TOC and biogenic silica content, was deposited [64]. This stage was short, but the scale of marine transgression was so large that most of the Yangtze platform was influenced, which makes it possible for the wide distribution of organic-enrich deposition on the lower Longmaxi Formation.

During early Aeronian, the uplift of Yangtze platform, together with marine regression, turned this region into a shallow shelf [27]. The sedimentation environment converted into oxic, thus, carbonate deposition resumed (Figures 4 and 5). The mutual dilution between detrital influx and carbonate minerals was evident, and ratio of fine to coarse detrital inputs was regulated by the fluctuation of sea level at this stage (CZ V–CZ XII, Figures 3 and 4). The TOC content was not high either due to the low preservation an productivity [64].

5.3. Identification of the Sweet Spot

Chemostratigraphy has played an important role, both for the exploration and development of shale gas, which provides not only the basis for stratigraphic correlation, but also the stratigraphic properties for evaluation [10,13,14]. Certain statistical surveys for the application of this method prove that 70% of the information needed for shale gas exploration can be provided by chemostratigraphic data [2]. For example, it can guide the conduction of horizontal drilling and provide much information for the fracturing of wells [3].

For sweet-spot identification, the basic protocol is that the rock should be both organic-rich and brittle. The TOC content is the best proxy for organic carbon, and the content of brittle minerals, for example quartz and carbonate, can be concluded from the geochemical data. Undoubtedly, the organic-rich chemozones of CZ I–CZ III (Wufeng Formation) and CZ IV (bottom of Longmaxi Formation), deposited under the anoxic environment, are thought to be potential sweet-spot layers for shale-gas exploration. Moreover, these successions belong to siliceous sediments, as well there being a thin carbonaceous layer of Guanyinqiao at the top of CZ III (Figure 4). The Si-Zr plot shows that there are two trends for Si, i.e., biogenic (Figure 7a,b) and detrital (Figure 7c). Zr is a typical detrital proxy, and the negative direction of Si-Zr relation shows a biogenic silica [42]. From this plot, one can find that most of the samples from CZ I–CZ IV are scattered along the biogenic trend line, indicating a significant contribution from the biogenic influx which is similar to that of typical shale gas in North America [3,9,13,14]. Namely, numerous brittle minerals are contained in successions, which is in favor of fracturing. Thus, chemozones of CZ I–CZ III (Wufeng Formation) and CZ IV (bottom of Longmaxi Formation) are both organic-

rich and brittle, which are beneficial sweet-spot layers for shale gas exploration. All this identification has been proven by the exploration and developed experience for shale-gas study of these two Formations [66].

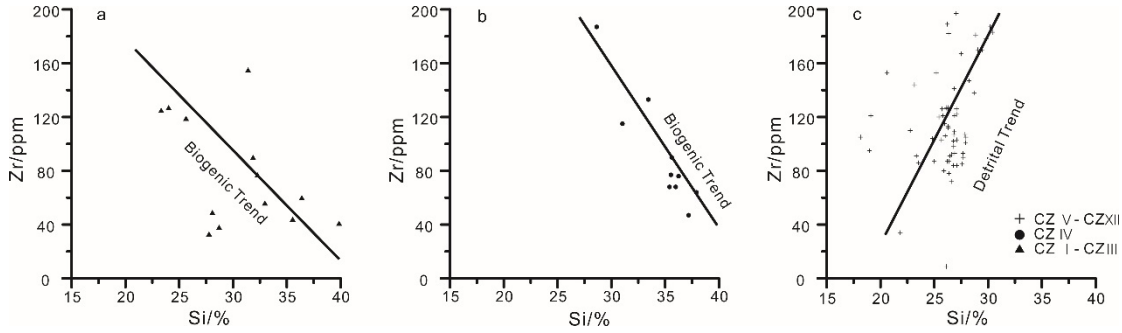


Figure 7. Si-Zr scatter plot of different chemozones along the Changning section. (**a**) Samples from the Wufeng Formation or CZ I–CZ III, (**b**) samples from the bottom of the Lower Longmaxi Formation or CZ IV, (**c**) samples from the Lower Longmaxi Formation or CZ V–CZ XII.

6. Conclusions

The chemostratigraphic technique presented in this paper has provided a convenient and reliable method for division of fine-grained successions. Two steps are involved for the implementation of this technique. Principal component analysis is firstly used for recognition of chemofacies defined by each elemental association. Then the unified chemozones can be acquired by the combination of chemozones from every chemofacies resulting from constrained clustering analysis. The main conclusions of this work are below:

1. Three chemofacies (or elemental associations) were proposed to optimally characterize the macroscopically homogeneous Wufeng-Longmaxi shales. The elemental association characterizing detrital inputs of the strata are K, Ti, Fe, Al, Na, Mg, Cr, Zr, Rb; the elemental association characterizing authigenic minerals are Ca, Sr, Mn, Si, S, Ba; the chemofacies characterizing redox-organic conditions are P, V, Ni, Zn, Cu, TOC.
2. The macroscopically homogeneous Wufeng-Longmaxi Formation shows geochemical heterogeneity from the perspective of detrital, authigenic, and redox-organic chemofacies, which enables the wide applicability of chemostratigraphy to the division and correlation of fine-grained strata.
3. Twelve chemozones were constructed for the sampled part of the Changning section, Sichuan of China. They are CZ I (0 m–3.0 m), CZ II (3.0 m–4.3 m), CZ III (4.3 m–8.8 m) for the Wufeng Formation, and CZ IV (8.8 m–33.6 m), CZ V (33.6 m–39.4 m), CZ VI (39.4 m–62.0 m), CZ VII (62.0 m–67.0 m), CZ VIII (67.0 m–72.6 m), CZ IX (72.6 m–98.8 m), CZ X (98.8 m–104.5 m), CZ XI (104.5 m–115.7 m), CZ XII (115.7 m–170 m) for the Longmaxi Formation. These chemozones not only correspond to the lithostratigraphic column perfectly but identify the boundaries that cannot be revealed by the latter.
4. A three-stage geochemical evolution along the Changning section was classified, coinciding approximately with the biostratigraphic stages [34], i.e., CZ (I–III) for Late Katian to Hirnaian, CZ IV for Rhuddanian, and CZ (V–XII) for Aeronian, respectively (Figure 6). Paleogeographic and paleoceanographic evolution of this region during the Late Ordovician to Early Silurian period were responsible for this evolution.
5. The organic-rich and brittle CZ I–IV were identified as preferable sweet-spot layers, as confirmed by the exploration experience.

Author Contributions: Conceptualization, Y.H. and C.W.; data curation, Z.Z.; formal analysis, Z.Z.; investigation, B.R. and X.L.; methodology, Z.Z. and Y.H.; resources, W.L.; supervision, Y.H. and C.W.; writing—original draft, Z.Z.; writing—review & editing, Y.H. All authors have read and agreed to the published version of the manuscript.

Funding: This research was jointly supported by the National Natural Science Foundation of China (Grant No. 41972112 and 41790455), the Fundamental Research Funds for the Central Universities of China (Grant No. 2652017224), and the China Geological Survey Program (DD20160207).

Institutional Review Board Statement: Not applicable.

Informed Consent Statement: Not applicable.

Data Availability Statement: The data presented in this study are available on request from the corresponding author.

Acknowledgments: The authors would like to thank the anonymous reviewers and editors for their valuable comments.

Conflicts of Interest: The authors declare no conflict of interest.

Appendix A

Table A1. The XRF results.

Sample	Thick	K	Ti	Fe	Al	Na	Mg	Ca	Si	TOC	S	Cr	Zr	Rb	Mn	Sr	Ba	P	V	Ni	Zn	Cu	V/Cr
	m	%	%	%	%	%	%	%	%	%	%	ppm	ppm	ppm	ppm	ppm	ppm	ppm	ppm	ppm	ppm	ppm	/
CN-78D	171.1	3.0	0.4	3.1	7.7	0.4	1.7	9.6	20.6	0.6	0.3	60.0	153.0	115.0	457.4	216.0	491.0	505.3	83.0	30.0	66.0	0.9	1.4
CN-77D	153.1	2.7	0.3	2.9	6.9	0.6	1.6	11.6	19.1	0.9	0.3	42.0	121.0	99.0	408.6	250.0	370.0	410.5	110.0	33.0	51.0	18.0	2.6
CN-76D	135.6	2.5	0.3	3.3	6.9	0.4	1.9	11.7	18.1	1.0	0.4	44.0	105.0	96.0	490.7	259.0	399.0	398.7	100.0	31.0	64.0	13.0	2.3
CN-75D	129.4	3.4	0.4	3.4	8.8	0.5	1.8	5.9	22.8	1.4	0.4	66.0	110.0	127.0	276.0	133.0	452.0	393.5	125.0	39.0	62.0	18.0	1.9
CN-74D	117.4	3.3	0.4	3.5	8.4	0.5	1.8	6.1	22.8	1.3	0.7	62.0	110.0	119.0	290.8	126.0	360.0	378.9	99.0	44.0	50.0	21.0	1.6
CN-73D	115.7	2.6	0.3	3.2	7.0	0.4	1.9	10.9	19.0	1.0	0.4	50.0	95.0	105.0	504.0	244.0	493.0	367.5	81.0	36.0	44.0	12.0	1.6
CN-72D	110.2	1.1	0.1	3.2	3.4	0.4	0.9	15.8	21.8	0.4	1.2	25.0	34.0	42.0	582.0	298.0	1590.0	273.1	43.0	21.0	55.0	0.9	1.7
CN-71D	104.5	3.4	0.4	3.7	8.9	0.5	1.9	4.9	23.5	1.2	0.6	64.0	86.0	134.0	274.7	100.0	508.0	322.9	123.0	50.0	65.0	12.0	1.9
CN-70D	98.8	3.2	0.4	3.5	8.3	0.5	1.8	5.7	23.3	1.4	0.6	64.0	91.0	112.0	321.8	112.0	320.0	374.2	117.0	58.0	175.0	30.0	1.8
CN-69D	93.1	3.4	0.4	3.8	9.0	0.5	1.7	3.3	25.0	2.1	0.7	74.0	87.0	134.0	232.3	90.0	427.0	397.4	115.0	46.0	65.0	27.0	1.6
CN-68D	87.1	3.3	0.4	3.7	8.6	0.6	1.7	3.2	25.9	1.7	0.4	64.0	80.0	135.0	260.4	72.0	477.0	399.0	106.0	40.0	83.0	23.0	1.7
CN-67D	86.6	3.4	0.4	3.5	8.8	0.5	1.7	2.6	26.6	1.5	0.3	68.0	72.0	135.0	212.0	58.0	424.0	423.3	96.0	28.0	59.0	25.0	1.4
CN-66D	86.1	3.3	0.4	3.6	8.8	0.5	1.7	1.7	27.6	1.4	0.3	71.0	85.0	134.0	157.7	50.0	450.0	424.8	109.0	35.0	72.0	27.0	1.5
CN-65D	85.6	3.3	0.4	3.8	8.9	0.5	1.8	2.1	27.1	0.9	0.4	62.0	84.0	135.0	195.8	55.0	386.0	384.2	118.0	39.0	103.0	32.0	1.9
CN-64D	85.1	3.4	0.4	3.7	9.1	0.6	1.8	2.5	26.2	1.1	0.4	70.0	87.0	137.0	213.3	65.0	382.0	403.1	115.0	41.0	88.0	28.0	1.6
CN-63D	84.6	3.5	0.4	3.8	9.1	0.6	1.8	1.9	26.8	1.3	0.3	70.0	84.0	146.0	189.3	52.0	326.0	412.4	114.0	46.0	78.0	25.0	1.6
CN-62D	84.1	3.1	0.4	3.7	8.7	0.6	1.9	3.3	25.7	1.3	0.4	67.0	103.0	122.0	306.3	82.0	353.0	378.1	114.0	37.0	99.0	25.0	1.7
CN-61D	83.6	3.4	0.4	3.7	9.1	0.5	1.8	2.6	26.1	1.2	0.0	7.1	8.8	14.5	241.8	6.5	55.3	369.5	10.2	3.6	6.7	2.6	1.4
CN-60D	83.1	3.1	0.4	3.8	8.5	0.6	1.9	4.0	24.8	1.2	0.4	64.0	104.0	123.0	469.9	98.0	398.0	383.1	118.0	39.0	101.0	16.0	1.8
CN-59D	82.6	3.4	0.4	3.7	9.0	0.5	1.8	2.4	26.4	1.4	0.5	73.0	78.0	135.0	236.9	61.0	313.0	392.5	116.0	38.0	62.0	24.0	1.6
CN-58D	82.1	3.4	0.4	3.7	9.2	0.6	1.8	1.8	26.8	1.5	0.2	66.0	102.0	144.0	180.8	52.0	588.0	435.2	106.0	34.0	88.0	26.0	1.6
CN-57D	81.6	3.3	0.4	3.7	8.9	0.5	1.8	2.4	26.9	1.2	0.4	59.0	93.0	114.0	214.9	56.0	182.0	432.2	104.0	40.0	112.0	21.0	1.8
CN-56D	81.1	3.3	0.4	3.6	8.8	0.5	1.7	1.9	27.7	1.2	0.4	72.0	93.0	138.0	197.6	50.0	534.0	391.1	97.0	38.0	45.0	24.0	1.3
CN-55D	80.6	3.3	0.4	3.5	8.9	0.5	1.7	1.5	27.9	1.4	0.4	63.0	105.0	128.0	176.8	47.0	396.0	413.0	101.0	37.0	88.0	19.0	1.6
CN-54D	80.1	3.3	0.4	3.6	9.0	0.5	1.7	1.7	27.9	1.2	0.3	64.0	107.0	136.0	196.8	52.0	348.0	424.5	106.0	40.0	65.0	23.0	1.7
CN-53D	79.6	3.3	0.4	3.6	8.8	0.5	1.8	2.4	26.8	1.1	0.3	66.0	98.0	134.0	270.1	68.0	528.0	384.9	102.0	40.0	118.0	21.0	1.5
CN-52D	79.1	3.3	0.4	3.5	8.9	0.5	1.8	1.7	27.7	0.7	0.3	63.0	90.0	140.0	217.7	49.0	552.0	409.9	92.0	42.0	63.0	21.0	1.5
CN-51D	78.6	3.9	0.3	3.1	10.6	0.5	1.7	1.4	26.8	0.8	0.1	31.0	107.0	133.0	154.2	41.0	374.0	286.1	48.0	19.0	80.0	9.6	1.5
CN-50D	78.1	3.2	0.4	3.5	8.7	0.5	1.7	1.8	27.9	2.0	0.4	59.0	101.0	125.0	205.2	54.0	351.0	391.0	88.0	36.0	46.0	14.0	1.5
CN-49D	77.6	3.4	0.4	4.1	9.2	0.4	1.8	1.9	26.3	1.4	0.4	68.0	87.0	137.0	298.6	45.0	380.0	440.9	98.0	43.0	80.0	22.0	1.4
CN-48D	77.1	3.2	0.4	3.5	8.8	0.5	1.8	2.6	27.1	1.1	0.2	60.0	122.0	129.0	288.1	72.0	428.0	404.7	90.0	39.0	62.0	14.0	1.5
CN-47D	76.6	3.2	0.4	3.7	8.9	0.6	1.9	2.5	26.9	0.9	0.4	68.0	121.0	123.0	249.2	68.0	489.0	438.2	90.0	34.0	75.0	14.0	1.3
CN-46D	75.8	3.3	0.4	3.8	9.2	0.6	1.8	2.2	26.9	1.3	0.3	62.0	109.0	124.0	244.6	58.0	368.0	407.9	98.0	41.0	79.0	21.0	1.6
CN-45D	75.1	3.3	0.4	3.8	8.8	0.7	1.7	3.0	26.0	1.0	0.7	74.0	106.0	125.0	300.5	71.0	271.0	386.3	106.0	42.0	52.0	18.0	1.4
CN-44D	74.3	3.5	0.4	3.7	9.3	0.7	1.8	1.9	26.4	1.7	0.5	60.0	91.0	144.0	201.0	48.0	533.0	416.1	109.0	42.0	64.0	17.0	1.8
CN-43D	73.5	3.3	0.4	3.5	9.0	0.6	1.8	2.3	27.1	1.6	0.3	57.0	126.0	128.0	250.3	66.0	374.0	387.5	78.0	34.0	68.0	14.0	1.4
CN-42D	73.1	3.4	0.4	3.8	9.2	0.7	1.8	1.6	27.1	1.4	0.3	68.0	103.0	142.0	208.4	46.0	567.0	407.9	109.0	54.0	97.0	27.0	1.6
CN-41D	72.6	3.3	0.4	3.8	8.8	0.4	1.7	2.7	26.6	1.0	0.3	55.0	92.0	121.0	381.0	65.0	36.0	402.2	97.0	2.3	51.0	23.0	1.8

Table A1. *Cont.*

Sample	Thick	K	Ti	Fe	Al	Na	Mg	Ca	Si	TOC	S	Cr	Zr	Rb	Mn	Sr	Ba	P	V	Ni	Zn	Cu	V/Cr
	m	%	%	%	%	%	%	%	%	%	%	ppm	ppm	ppm	ppm	ppm	ppm	ppm	ppm	ppm	ppm	ppm	/
CN-40D	72.2	3.1	0.4	3.5	8.6	0.5	1.7	3.4	26.2	0.9	0.7	57.0	126.0	128.0	300.5	90.0	468.0	393.2	99.0	46.0	528.0	23.0	1.7
CN-39D	71.8	3.2	0.4	3.6	8.7	0.5	1.7	3.3	26.3	1.1	0.4	60.0	127.0	128.0	284.2	83.0	456.0	417.2	100.0	50.0	138.0	23.0	1.7
CN-38D	71.1	3.2	0.4	3.7	8.9	0.6	1.8	3.1	26.3	1.4	0.5	58.0	113.0	122.0	255.9	74.0	300.0	436.4	96.0	45.0	64.0	22.0	1.7
CN-37D	70.6	3.0	0.4	3.6	8.6	0.6	1.9	4.1	25.4	0.7	0.4	60.0	120.0	106.0	396.7	85.0	210.0	432.3	86.0	37.0	87.0	16.0	1.4
CN-36D	70.1	3.3	0.4	3.6	9.0	0.6	1.8	3.2	26.0	1.0	0.5	66.0	115.0	131.0	269.5	79.0	405.0	415.5	94.0	39.0	53.0	14.0	1.4
CN-35D	69.6	3.2	0.4	3.6	8.8	0.6	1.8	3.7	25.7	1.1	0.5	68.0	126.0	120.0	350.3	89.0	331.0	421.4	87.0	39.0	59.0	10.0	1.3
CN-34D	69.1	3.3	0.4	3.6	8.9	0.6	1.7	3.2	26.1	1.2	0.4	60.0	127.0	134.0	286.4	74.0	477.0	416.2	94.0	45.0	87.0	21.0	1.6
CN-33D	68.6	3.4	0.4	3.5	9.1	0.5	1.7	2.7	26.3	1.2	0.5	61.0	112.0	133.0	240.9	72.0	494.0	402.1	92.0	42.0	47.0	14.0	1.5
CN-32D	68.1	3.3	0.4	3.5	9.1	0.6	1.8	2.4	26.8	0.3	0.5	70.0	141.0	133.0	247.5	63.0	481.0	426.1	97.0	47.0	83.0	9.6	1.4
CN-31D	67.6	3.2	0.4	3.6	8.8	0.5	1.8	3.3	25.8	1.3	0.3	70.0	121.0	125.0	388.3	78.0	374.0	377.8	88.0	39.0	63.0	14.0	1.3
CN-30D	67.0	3.2	0.4	3.6	8.8	0.5	1.8	3.3	25.8	1.1	0.3	70.0	121.0	125.0	388.3	78.0	374.0	377.8	88.0	39.0	63.0	14.0	1.3
CN-29D	65.6	3.5	0.4	3.3	9.5	0.4	1.5	0.1	28.2	1.5	0.5	67.0	147.0	140.0	76.2	30.0	352.0	381.6	104.0	28.0	47.0	14.0	1.6
CN-28D	65.1	3.1	0.4	3.3	9.1	0.7	1.6	0.2	28.8	0.3	0.8	57.0	181.0	117.0	95.0	36.0	437.0	494.8	85.0	44.0	58.0	19.0	1.5
CN-27D	64.7	3.4	0.4	2.6	9.3	0.5	1.3	0.1	28.7	1.5	0.1	74.0	138.0	123.0	66.7	27.0	298.0	212.8	101.0	31.0	53.0	0.9	1.4
CN-26D	64.3	3.4	0.4	2.3	9.4	0.7	1.3	0.2	30.2	1.2	0.0	74.0	187.0	132.0	95.3	36.0	394.0	314.7	88.0	28.0	54.0	0.9	1.2
CN-25D	63.8	3.4	0.4	2.8	9.5	0.6	1.5	0.2	29.5	1.2	0.2	62.0	170.0	127.0	66.7	33.0	358.0	212.7	101.0	20.0	33.0	1.3	1.6
CN-24D	63.4	3.4	0.4	3.2	9.5	0.5	1.5	0.1	29.0	0.9	0.4	65.0	170.0	129.0	85.7	31.0	335.0	295.5	97.0	31.0	36.0	0.9	1.5
CN-23D	62.9	3.4	0.4	2.3	9.3	0.5	1.3	0.2	30.4	1.3	0.0	60.0	183.0	132.0	76.2	33.0	517.0	139.4	74.0	19.0	38.0	0.9	1.2
CN-22D	62.5	3.3	0.4	2.0	9.1	0.6	1.1	0.1	30.3	1.4	0.4	59.0	187.0	134.0	57.1	32.0	443.0	123.2	71.0	11.0	18.0	10.0	1.2
CN-21D	62.0	3.3	0.4	2.9	8.9	0.7	1.3	0.1	29.8	1.6	0.4	71.0	178.0	126.0	66.5	36.0	370.0	517.3	95.0	20.0	31.0	3.0	1.3
CN-20D	39.4	3.2	0.4	3.4	8.7	0.6	1.7	2.4	27.5	1.3	0.5	60.0	167.0	123.0	182.5	64.0	485.0	437.5	83.0	38.0	86.0	21.0	1.4
CN-19D	38.3	2.7	0.4	3.3	7.8	0.8	1.7	3.8	27.0	1.9	0.4	52.0	197.0	104.0	337.6	94.0	346.0	479.8	79.0	36.0	73.0	17.0	1.5
CN-18D	37.1	2.7	0.4	3.0	7.8	0.9	1.7	4.6	26.3	1.2	0.6	58.0	182.0	104.0	279.1	116.0	402.0	449.4	77.0	41.0	76.0	16.0	1.3
CN-17D	36.1	2.7	0.4	3.0	7.8	0.9	1.7	4.8	26.2	1.2	0.6	49.0	189.0	104.0	265.8	119.0	422.0	450.2	77.0	46.0	61.0	21.0	1.6
CN-16D	35.3	2.4	0.3	3.7	7.2	0.8	2.0	7.4	23.2	1.2	0.2	46.0	144.0	89.0	674.3	198.0	308.0	461.4	69.0	31.0	38.0	12.0	1.5
CN-15D	34.6	2.9	0.4	3.6	8.3	0.7	1.8	4.6	25.2	1.2	0.2	57.0	153.0	113.0	475.2	103.0	409.0	536.3	77.0	33.0	59.0	22.0	1.4
CN-14D	33.6	3.0	0.4	3.4	8.5	0.9	1.6	1.9	28.6	1.3	0.1	56.0	187.0	112.0	123.3	58.0	329.0	521.6	77.0	35.0	101.0	18.0	1.4
CN-13-8D	25.8	1.5	0.2	1.2	3.4	0.3	0.3	0.0	37.9	3.1	0.1	29.0	64.0	53.0	7.7	14.0	273.0	392.9	231.0	49.0	25.0	22.0	8.0
CN-13-7D	23.8	1.8	0.2	1.5	3.9	0.4	0.4	0.1	35.6	3.5	0.9	40.0	90.0	71.0	18.6	23.0	390.0	457.1	337.0	91.0	46.0	22.0	8.4
CN-13-6D	21.8	1.6	0.2	1.4	3.7	0.4	0.3	0.1	36.2	4.1	0.9	37.0	76.0	61.0	18.6	20.0	450.0	551.5	299.0	79.0	56.0	26.0	8.1
CN-13-5D	19.8	1.6	0.2	1.3	3.5	0.4	0.4	0.6	36.0	3.9	0.9	34.0	68.0	61.0	92.9	31.0	451.0	461.1	264.0	101.0	46.0	42.0	7.8
CN-13-4D	17.8	2.7	0.3	2.6	3.7	0.2	0.3	0.5	33.4	5.5	1.5	67.0	133.0	127.0	100.1	47.0	1030.0	861.2	516.0	214.0	65.0	66.0	7.7
CN-13-3D	15.8	1.7	0.2	1.6	3.7	0.4	0.5	0.5	35.4	4.2	1.1	39.0	68.0	69.0	83.7	30.0	607.0	367.7	362.0	129.0	32.0	50.0	9.3
CN-13-2D	13.8	1.8	0.2	1.6	3.7	0.4	0.3	0.1	35.5	4.6	1.1	44.0	77.0	69.0	37.2	26.0	395.0	515.3	300.0	112.0	43.0	35.0	6.8
CN-13-1D	11.8	2.4	0.3	2.1	5.4	0.6	0.5	0.1	31.0	6.5	1.5	68.0	115.0	101.0	37.5	35.0	527.0	624.2	529.0	125.0	47.0	39.0	7.8
CN-13D	8.8	1.2	0.1	0.7	3.0	0.0	0.3	0.1	37.2	7.1	0.1	42.0	47.0	45.0	13.9	9.3	202.0	202.8	388.0	86.0	80.0	2.0	9.2
CN-12D	7.8	1.7	0.3	1.9	4.5	0.5	1.1	10.3	23.3	3.4	1.4	39.0	125.0	73.0	353.8	230.0	279.0	892.7	208.0	146.0	177.0	58.0	5.3
CN-11D	6.6	1.8	0.3	2.0	4.6	0.5	1.0	9.8	24.0	3.1	1.1	35.0	127.0	68.0	365.0	212.0	311.0	910.8	208.0	145.0	199.0	62.0	5.9
CN-10D	5.3	1.8	0.3	1.8	4.6	0.5	1.0	8.1	25.6	3.9	1.2	49.0	119.0	73.0	298.1	161.0	249.0	745.6	220.0	152.0	182.0	61.0	4.5
CN-9D	4.3	2.6	0.3	2.5	6.4	0.4	0.8	0.2	31.4	3.6	0.2	65.0	155.0	109.0	37.6	25.0	485.0	914.4	353.0	194.0	386.0	47.0	5.4
CN-8D	3.9	1.3	0.2	2.6	3.7	0.3	0.4	0.4	31.9	9.8	0.1	31.0	90.0	44.0	64.9	19.0	103.0	1534.1	166.0	221.0	416.0	161.0	5.4
CN-7D	3.4	1.8	0.2	4.0	4.0	0.1	0.5	0.1	32.3	7.7	0.1	48.0	77.0	68.0	37.0	9.3	143.0	589.7	156.0	165.0	347.0	33.0	3.3

Table A1. *Cont.*

Sample	Thick	K	Ti	Fe	Al	Na	Mg	Ca	Si	TOC	S	Cr	Zr	Rb	Mn	Sr	Ba	P	V	Ni	Zn	Cu	V/Cr
	m	%	%	%	%	%	%	%	%	%	%	ppm	ppm	ppm	ppm	ppm	ppm	ppm	ppm	ppm	ppm	ppm	/
CN-6D	3.0	1.4	0.2	1.8	3.6	0.2	0.5	0.3	36.4	4.8	0.2	47.0	60.0	62.0	35.3	33.0	246.0	664.1	179.0	95.0	191.0	60.0	3.8
CN-5D	2.5	1.0	0.1	1.0	2.5	0.1	0.8	10.8	27.8	2.2	0.4	36.0	33.0	37.0	437.5	222.0	214.0	428.9	122.0	49.0	34.0	23.0	3.4
CN-4D	2.0	1.3	0.2	1.5	3.2	0.2	0.7	4.5	33.0	1.8	0.2	46.0	56.0	53.0	262.5	82.0	276.0	520.7	166.0	63.0	63.0	42.0	3.6
CN-3D	1.5	1.1	0.1	1.1	2.9	0.1	0.3	0.1	39.9	0.8	0.0	36.0	41.0	37.0	21.3	10.0	104.0	522.9	117.0	63.0	174.0	97.0	3.3
CN-2D	1.0	1.2	0.1	1.3	3.1	0.1	0.7	3.1	35.5	1.8	0.2	41.0	44.0	43.0	168.3	47.0	204.0	416.1	131.0	64.0	179.0	56.0	3.2
CN-1D	0.5	1.6	0.2	1.9	4.1	0.1	1.4	7.0	28.1	2.7	0.1	57.0	49.0	56.0	378.9	91.0	134.0	422.0	183.0	72.0	149.0	54.0	3.2
CN-0D	0.0	1.1	0.1	1.2	2.7	0.1	1.3	8.8	28.7	2.7	0.2	39.0	38.0	43.0	498.0	149.0	209.0	297.7	119.0	40.0	72.0	38.0	3.1

Appendix B

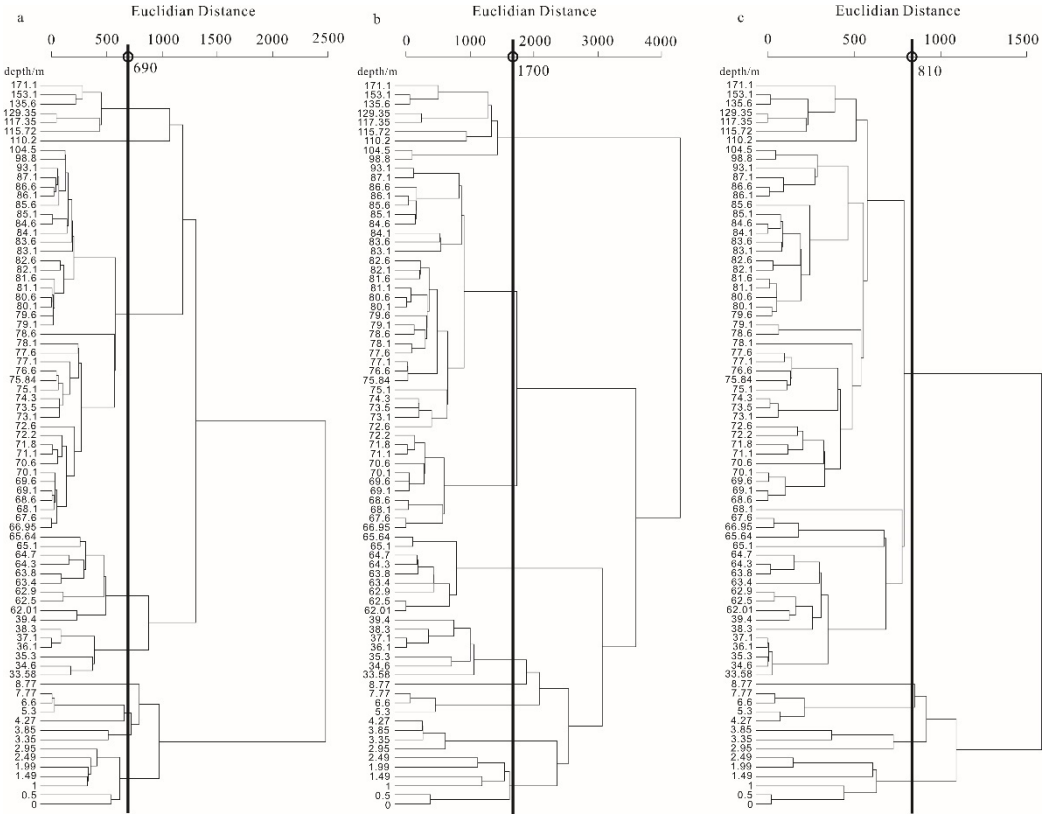


Figure A1. The dendrograms of constrained clustering analysis (**a**) derived from detrital chemofacies; (**b**) from authigenic chemofacies; and (**c**) from redox-organic chemofacies.

References

1. Curtis, J.B. Fractured shale–gas systems. *AAPG Bull.* **2002**, *86*, 1921–1938.
2. Slatt, R.M.; Rodriguez, N.D. Comparative sequence stratigraphy and organic geochemistry of gas shales: Commonality or coincidence? *J. Nat. Gas Sci. Eng.* **2012**, *8*, 68–84. [CrossRef]
3. Ratcliffe, K.T.; Wright, A.M.; Schmidt, K. Application of inorganic whole–rock geochemistry to shale resource plays: An example from the Eagle Ford Shale Formation, Texas. *Sediment. Rec.* **2012**, *10*, 4–9. [CrossRef]
4. Zhai, G.Y.; Li, J.; Jiao, Y.; Wang, Y.F.; Liu, G.H.; Xu, Q.; Wang, C.; Chen, R.; Guo, X.B. Applications of chemostratigraphy in a characterization of shale gas Sedimentary Microfacies and predictions of sweet spots—Taking the Cambrian black shales in Western Hubei as an example. *Mar. Pet. Geol.* **2019**, *109*, 547–560. [CrossRef]
5. Turner, B.W.; Tréanton, J.A.; Slatt, R.M. The use of chemostratigraphy to refine ambiguous sequence stratigraphic correlations in marine mudrocks. An example from the Woodford Shale, Oklahoma, USA. *J. Geol. Soc. Lond.* **2016**, *173*, 854–868. [CrossRef]
6. Picard, M.D. Classification of fine-grained sedimentary rocks. *J. Sediment. Res.* **1971**, *41*, 179–195.
7. Abouelresh, M.O.; Slatt, R.M. Lithofacies and sequence stratigraphy of the Barnett Shale in east-central Fort Worth Basin, Texas. *AAPG Bull.* **2012**, *96*, 1–22. [CrossRef]
8. Chen, L.; Lu, Y.C.; Jiang, S.; Li, J.Q.; Guo, T.L.; Luo, C. Heterogeneity of the Lower Silurian Longmaxi marine shale in the southeast Sichuan Basin of China. *Mar. Pet. Geol.* **2015**, *65*, 232–246. [CrossRef]
9. Turner, B.W.; Molinares-Blanco, C.E.; Slatt, R.M. Chemostratigraphic, palynostratigraphic, and sequence stratigraphic analysis of the Woodford Shale, Wyche, Farm Quarry, Pontotoc County, Oklahoma. *Interpretation* **2015**, *3*, SH1–SH9. [CrossRef]
10. Turner, B.W. Utilization of Chemostratigraphic Proxies for Generating and Refining Sequence Stratigraphic Frameworks in Mudrocks and Shales. Ph.D. Dissertation, University of Oklahoma, Norman, OK, USA, 2016.
11. Pearce, T.J.; Besly, B.M.; Wray, D.S.; Wright, D.K. Chemostratigraphy: A method to improve interwell correlation in barren sequences-a case study using onshore Duckmantian/Stephanian sequences (West Midlands, U.K.). *Sediment. Geol.* **1999**, *124*, 197–220. [CrossRef]

12. Ramkumar, M.; Berner, Z.; Stüben, D. Hierarchical delineation and multivariate statistical discrimination of chemozones of the Cauvery Basin, south India: Implications on spatio-temporal scales of stratigraphic correlation. *Pet. Sci.* **2010**, *7*, 435–447. [CrossRef]
13. Ratcliffe, K.T.; Martin, J.; Pearce, T.J.; Hughes, A.D.; Lawton, D.E.; Wray, D.S.; Bessa, F. A regional chemostratigraphically-defined correlation framework for the late Triassic TAG-I Formation in Blocks 402 and 405a, Algeria. *Petrol. Geosci.* **2006**, *12*, 3–12. [CrossRef]
14. Ratcliffe, K.T.; Wilson, A.; Payenberg, T.; Rittersbacher, A.; Hildred, G.V.; Flint, S.S. Ground truthing chemostratigraphic correlations in fluvial systems. *AAPG Bull.* **2015**, *99*, 155–180. [CrossRef]
15. Ikhane, P.R.; Akintola, A.I.; Bankole, S.I.; Ajibade, O.M.; Edward, O.O. Chemostratigraphic characterization of siliciclastic Rocks in parts of the eastern Dahomey Basin, Southwestern Nigeria. *J. Geogr. Geol.* **2014**, *6*, 88–108.
16. Rowe, H.; Hughes, N.; Robinson, K. The quantification and application of and held energy-dispersive x-ray fluorescence (ED-XRF) in mudrock chemostratigraphy and geochemistry. *Chem. Geol.* **2012**, *324–325*, 122–131. [CrossRef]
17. Asiedu, D.K.; Suzuki, S.; Nogami, K.; Shibata, T. Geochemistry of Lower Cretaceous sediments, inner zone of southwest Japan: Constraints on provenance and tectonic environment. *Geochem. J.* **2000**, *34*, 155–173. [CrossRef]
18. Dypvik, H.; Harris, N.B. Geochemical facies analysis of fine-grained siliciclastics using Th/U, Zr/Rb and (Zr+Rb)/Sr ratios. *Chem. Geol.* **2001**, *181*, 131–146. [CrossRef]
19. Weissert, H.; Joachimski, M.; Sarnthein, M. Chemostratigraphy. *Newsl. Stratigr.* **2008**, *42*, 145–179. [CrossRef]
20. Montero-Serrano, J.C.; Palarea-Albaladejo, J.; Martín-Fernández, J.A.; Martínez-Santana, M.; Gutiérrez-Martín, J.V.G. Sedimentary chemofacies characterization by means of multivariate analysis. *Sediment. Geol.* **2010**, *228*, 218–228. [CrossRef]
21. Abu-Ali, R.; El-Kammar, A.; Kuss, J. Chemostratigraphy of the Upper Cretaceous-Paleogene organic-rich succession on the southern Tethys margin in Egypt. *J. Afr. Earth Sci.* **2020**, *164*, 103779. [CrossRef]
22. Zhang, J.C.; Xu, B.; Nie, H.K.; Wang, Z.Y.; Lin, T. Exploration potential of shale gas resources in China. *Nat. Gas Ind.* **2008**, *28*, 136–140.
23. Chen, S.B.; Zhu, Y.M.; Wang, H.Y.; Liu, H.L.; Wei, W.; Fang, J.H. Shale gas reservoir characterisation: A typical case in the southern Sichuan Basin of China. *Energy* **2011**, *36*, 6609–6616. [CrossRef]
24. Liang, C.; Jiang, Z.X.; Yang, Y.T.; Wei, X.J. Shale lithofacies and reservoir space of the Wufeng–Longmaxi Formation, Sichuan Basin, China. *Pet. Explor. Dev.* **2012**, *39*, 736–743. [CrossRef]
25. Chen, X.; Bergström, S.M.; Zhang, Y.D.; Wang, Z.H. A regional tectonic event of Katian (Late Ordovician) age across three major blocks of China. *Chin. Sci. Bull.* **2013**, *58*, 4292–4299. [CrossRef]
26. Liu, S.G.; Wang, S.Y.; Sun, W.; Ran, B.; Yang, D.; Luo, C.; Ye, Y.H.; Bai, Z.Q.; Qiu, J.W.; Zhang, X. Characteristics of black shale in Wufeng Formation and Longmaxi Formation in Sichuan Basin and its peripheral areas. *J. Chengdu Univ. Technol. Sci. Technol. Ed.* **2013**, *40*, 622–638.
27. Zhou, K.K. Middle Ordovician-Early Silurian Lithofacies Paleogeography of Middle-Upper Yangtze and Its Southeastern Margin. Ph.D. Dissertation, Chinese Academy of Geological Sciences, Beijing, China, 2015.
28. Guo, H.Y.; Li, Z.F.; Li, D.H.; Zhang, T.M.; Wang, Z.C.; Yu, J.F. Lithofacies palaeogeography of the Early Silurian in Sichuan area. *J. Palaeogeogr.* **2004**, *6*, 20–29.
29. Wang, G.P.; Jin, Z.J.; Liu, G.X.; Liu, Q.Y.; Liu, Z.B.; Wang, H.L.; Liang, X.P.; Jiang, T.; Wang, R.Y. Geological implications of gamma ray (GR) anomalies in marine shales: A case study of the Ordovician-Silurian Wufeng-Longmaxi succession in the Sichuan Basin and its periphery, Southwest China. *J. Asian Earth Sci.* **2020**, *199*, 104359. [CrossRef]
30. Haq, B.U.; Schutter, S.R. A chronology of Paleozoic sea-level changes. *Science* **2008**, *322*, 64–68. [CrossRef] [PubMed]
31. Brenchley, P.J.; Newall, G. A facies analysis of upper Ordovician regressive sequences in the Oslo Region, Norway—A record of glacio-eustatic changes. *Palaeogeogr. Palaeoclimatol. Palaeoecol.* **1980**, *31*, 1–38. [CrossRef]
32. Jin, Z.; Nie, H.; Liu, Q.; Zhao, J.; Jiang, T. Source and seal coupling mechanism for shale gas enrichment in upper Ordovician Wufeng Formation—Lower Silurian Longmaxi Formation in Sichuan Basin and its periphery. *Mar. Petrol. Geol.* **2018**, *97*, 78–93. [CrossRef]
33. Luo, C.; Wang, L.S.; Shi, X.W.; Zhang, J.; Wu, W.; Zhao, S.X. Biostratigraphy of the Wufeng to Longmaxi Formation at well Ning 211 of Changning shale gas field. *J. Stratigr.* **2017**, *41*, 142–152.
34. Duan, W.Z. Graptolite Biostratigraphy and Carbon Isotope Stratigraphy of Upper Ordovicain–Lower Silurian in Changning, Sichuan, China. Ph.D. Dissertation, China University of Geoscience, Beijing, China, 2011.
35. Craigie, N.W. Applications of chemostratigraphy in Cretaceous sediments encountered in the North Central Rubal-Khali Basin, Saudi Arabia. *J. Afr. Earth Sci.* **2015**, *104*, 27–42. [CrossRef]
36. Reategui, K.; Martinez, M.; Esteves, I.; Gutierrez, J.V.; Martinez, A.; Melendez, W.; Urbanzi, F. Geochemistry of the Mirador Formation (Late Eocene-Early Oligocene), southwestern Venezuela: Chemostratigraphic constraints on provenance and the influence of the sea level. *Geochem. J.* **2005**, *39*, 213–226. [CrossRef]
37. Reyment, R.A. A quantitative procedure for chemostratigraphy. *Stratigraphy* **2004**, *1*, 103–104.
38. Gill, D.; Shomrony, A.; Fligelman, H. Numerical zonation of Log suites and Log facies recognition by multivariate clustering. *AAPG Bull.* **1993**, *77*, 1781–1791.
39. Reyment, R.A. Multiple Group Principal Component Analysis. *Math. Geol.* **1997**, *29*, 1–16. [CrossRef]

40. Svendsen, J.; Friis, H.; Stollhoften, H.; Hartley, N. Facies discrimination in a mixed fluvio-eolian setting using elemental whole-rock geochemistry-applications for reservoir characterization. *J. Sediment. Res.* **2007**, *77*, 23–33. [CrossRef]
41. Algeo, T.J.; Maynard, J.B. Trace-element behavior and redox facies in core shales of Upper Pensylvanian Kansas-type cyclothems. *Geochem. J.* **2004**, *206*, 289–318.
42. Sageman, B.B.; Lyons, T.W. Geochemistry of Fine-grained Sediments and Sedimentary Rocks. *Treatise Geochem.* **2003**, *7*, 115–158.
43. Žibret, G.; Šajn, R. Hunting for geochemical associations of elements: Factor analysis and self-organising maps. *Math. Geosci.* **2010**, *42*, 681–703. [CrossRef]
44. Figueroa-Cisterna, J.; Bagur-González, M.G.; Morales-Ruano, S.; Carrillo-Rosúa, J.; Martín-Peinado, F. The use of a combined portable X ray fluorescence and multivariate statistical methods to assess a validated macroscopic rock samples classification in an ore exploration survey. *Talanta* **2011**, *85*, 2307–2315. [CrossRef] [PubMed]
45. Montilla, L.A.; Martínez, M.; Márquez, G.; Escobar, M.; Sierra, C.; Gallego, J.R.; Esteves, I.; Gutiérrez, J.V. Geochemistry and chemostratigraphy of the Colón-Mito Juan units (Campanian-Maastrichtian), Venezuela: Implications for provenance, depositional conditions, and stratigraphic subdivision. *Geochem. J.* **2013**, *47*, 537–546. [CrossRef]
46. Ward, E.H. Hierarchical grouping to optimize an objective function. *J. Am. Stat. Assoc.* **1963**, *58*, 236–244. [CrossRef]
47. Templ, M.; Filzmoser, P.; Reimann, C. Cluster analysis applied to regional geochemical data: Problems and possibilities. *Appl. Geochem.* **2008**, *23*, 2198–2213. [CrossRef]
48. Bennett, K.D. Determination of the number of zones in a biostratigraphical sequence. *New Phytol.* **1996**, *132*, 155–170. [CrossRef]
49. Martín-Fernández, J.A.; Barceló-Vidal, C.; Pawlowsky-Glahn, V. Dealing with zeros and missing values in compositional data sets using nonparametric imputation. *Math. Geol.* **2003**, *35*, 253–278. [CrossRef]
50. Rousseeuw, P.J.; Driessen, K.V. A fast algorithm for the minimum covariance determinant estimator. *Technometrics* **1999**, *41*, 212–223. [CrossRef]
51. Tribovillard, N.; Algeo, T.J.; Lyons, T.; Riboulleau, A. Trace metals as paleoredox and paleoproductivity proxies: An update. *Chem. Geol.* **2006**, *232*, 12–32. [CrossRef]
52. Pearce, T.J.; Jarvis, I. Applications of geochemical data to modelling sediment dispersal patterns in distal turbidites: Late Quaternary of the Madeira Abyssal Plain. *J. Sediment. Res.* **1992**, *62*, 1112–1129.
53. Banner, J.L. Application of the trace element and isotope geochemistry of strontium to studies of carbonate diagenesis. *Sedimentology* **1995**, *42*, 805–824. [CrossRef]
54. Föllmi, K.B. The phosphorus cycle, phosphogenesis and marine phosphate-rich deposits. *Earth-Sci. Rev.* **1996**, *40*, 55–124. [CrossRef]
55. Huang, Y.J.; Wang, C.S.; Chen, X. Response of reactive phosphorus burial to the sedimentary transition from Cretaceous black shales to oceanic red beds in Southern Tibet. *Acta Geol. Sin. (Engl. Ed.)* **2007**, *81*, 1012–1018.
56. Jenkyns, H.C. Geochemistry of oceanic anoxic events. *Geochem. Geophys. Geosyst.* **2010**, *11*, 427–428. [CrossRef]
57. Morse, J.W.; Luther, G.W. Chemical influences on trace metal-sulfide interactions in anoxic sediments. *Geochim. Cosmochim. Acta* **1999**, *63*, 3373–3378. [CrossRef]
58. Calvert, S.E.; Pedersen, T.F. Geochemistry of recent oxic and anoxic sediments: Implications for the geological record. *Mar. Geol.* **1993**, *113*, 67–88. [CrossRef]
59. Fernex, F.; Février, G.; Bénaïm, J.; Arnoux, A. Copper, lead and zinc trapping in Mediterranean deep-sea sediments: Probable coprecipitation with Mn and Fe. *Chem. Geol.* **1992**, *98*, 293–306. [CrossRef]
60. Wang, S.F.; Dong, D.Z.; Wang, Y.M.; Huang, J.L.; Pu, B.L. Geochemistry evaluation index of redox-sensitive elements for depositional environments of Silurian Longmaxi organic-rich shale in the south of Sichuan basin. *Mar. Orig. Pet. Geol.* **2014**, *19*, 27–34.
61. Dong, D.Z.; Cheng, K.M.; Wang, Y.M.; Li, X.J.; Wang, S.J.; Huang, J.L. Forming conditions and characteristics of shale gas in Lower Paleozoic of Upper Yangtze region, China. *Oil Gas Geol.* **2010**, *31*, 288–299.
62. Zhang, C.M.; Jiang, Z.X.; Guo, H.Y.; Zhang, W.S. Geochemical characteristics and paleoenvironment reconstruction of the Longmaxi Formation in southeast Sichuan and northern GuiZhou. *Geol. Sci. Technol. Inf.* **2013**, *32*, 124–130.
63. Jones, B.; Manning, D.A.C. Comparison of geochemical indices used for the interpretation of paleoredox conditions in ancient mudstones. *Chem. Geol.* **1994**, *111*, 111–129. [CrossRef]
64. Yan, D.T.; Chen, D.Z.; Wang, Q.C.; Wang, J.G. Predominance of stratified anoxic Yangtze Sea interrupted by short-term oxygenation during the Ordo-Silurian transition. *Chem. Geol.* **2012**, *291*, 69–78. [CrossRef]
65. Johnson, M.E.; Rong, J.Y.; Yang, X.C. Intercontinental correlation by sea-level events in the Early Silurian of North America and China (Yangtze Platform). *Geol. Soc. Am. Bull.* **1985**, *96*, 1384–1397. [CrossRef]
66. Abouelresh, M.O.; Slatt, R.M. Shale Depositional Processes: Example from the Paleozoic Barnett Shale, Fort Worth Basin, Texas, USA. *Cent. Eur. J. Geosci.* **2011**, *3*, 398–409. [CrossRef]